NANO · MICRO small
www.small-journal.com

Carbon Nanotubes Enabling Highly Efficient Cell Apoptosis by Low-Intensity Nanosecond Electric Pulses via Perturbing Calcium Handling

Zheng Mao, Youyu Zhang, Nan Lu, Shun Cheng, Ronghan Hong, and Qing Huo Liu**

Effective induction of targeted cancer cells apoptosis with minimum side effects has always been the primary objective for anti-tumor therapy. In this study, carbon nanotubes (CNTs) are employed for their unique ability to target tumors and amplify the localized electric field due to the high aspect ratio. Highly efficient and cancer cell specific apoptosis is finally achieved by combining carbon nanotubes with low intensity nanosecond electric pulses (nsEPs). The underlying mechanism may be as follows: the electric field produced by nsEPs is amplified by CNTs, causing an enhanced plasma membrane permeabilization and Ca^{2+} influx, simultaneously triggering Ca^{2+} release from intracellular storages to cytoplasm in a direct/indirect manner. All the changes above lead to excessive mitochondrial Ca^{2+} uptake. Substructural damage and obvious mitochondria membrane potential depolarization are caused subsequently with the combined action of numerously reactive oxygen species production, ultimately initiating the apoptotic process through the translocation of cytochrome c to the cytoplasm and activating apoptotic markers including caspase-9 and -3. Thus, the combination of nanosecond electric field with carbon nanotubes can actually promote HCT116 cell death via mitochondrial signaling pathway-mediated cell apoptosis. These results may provide a new and highly efficient strategy for cancer therapy.

1. Introduction

Techniques to apply electric pulses to biological cells to induce different cellular responses have been developed for many medical applications.[1,2] The process, called electroporation or electropermeabilization, is strongly affected by the duration and the intensity of the applied electric field. Milli- and microsecond pulses with an amplitude of several kV cm^{-1} are traditionally used to generate pores in the outer cell membrane, which can be repaired shortly after the exposure.[3] This reversible electroporation, allowing the transit of the molecules including drugs, genes, nanoparticles and so on into the cell, is commonly used for gene therapy and targeted electrochemotherapy.[4–7] In recent decades, nanosecond electric pulse (nsEP) has been widely employed to penetrate the plasma membrane and obtain responses from cell interior without thermal effects.[8–10] These special features make nsEPs promising tools for diverse biomedical applications, especially, for the induction of cell apoptosis instead of necrosis in cancer therapy.[11–13] Currently, needle electrodes and flat plate electrodes are used to transmit the electric field from a pulse generator to the target tissue. However, either a limited coverage of the electric field or an unexpected wide-spread cell damages induced by the high field intensity can result in relatively low antitumor therapy efficacy. In addition, a strong electric field strength up to several hundreds of kV cm^{-1} is required.[14,15] Due to the limitation of hardware techniques, such a high field is not easy to be realized. Thus, some supplementary modalities are needed.

Carbon nanotubes (CNTs), a kind of novel carbon allotrope, are found to have field emission capability because of their high aspect ratio and good conductivity (metallic CNTs and some of the semiconducting MWNTs with large diameter[16]). The special electronic properties allow CNTs to enhance the electric field around their tips and then form a localized high field region.[17,18] So, when applied to biomedicine, stronger cell electroresponses are achieved by combining CNTs with low intensity electric pulses.[19–24] On the other hand, via both passive and active pathways, carbon nanotubes were reported to be cancer-targeted and they were demonstrated to exhibit a high levels of tumor uptake.[25,26] Considering these promising properties, in this study, CNTs were employed in combination with low intensity nsEPs stimulation in vitro to sufficiently increase human colon cancer cells mortality. And results showed that

Z. Mao, Dr. Y. Zhang, N. Lu, S. Cheng, R. Hong
Institute of Electromagnetics and Acoustics and Key Laboratory of Electromagnetic Wave Science and Detection Technology
Xiamen University
Xiamen 361005, China
E-mail: zhangyouyu@xmu.edu.cn
Dr. Y. Zhang
Shenzhen Research Institute of Xiamen University
Shenzhen 518000, China
Prof. Q. H. Liu
Department of Electrical and Computer Engineering
Duke University
Durham, NC 27708, USA
E-mail: qhliu@duke.edu
The ORCID identification number(s) for the author(s) of this article can be found under https://doi.org/10.1002/smll.201904047.

DOI: 10.1002/smll.201904047

combination treatment with CNTs and nsEPs was able to induce highly efficient cell apoptosis.

Apoptosis, also known as programmed cell death, is a complex and sophisticated process. Several major signaling pathways have been shown to be associated with apoptosis in mammalian cells.[27–29] Mitochondria, crucial regulators of the intrinsic pathway of apoptosis, can be considered as the prime target of inducing tumor cells apoptosis. In cancer cells, the mitochondria-mediated apoptotic pathway is suppressed by the overexpression of antiapoptotic proteins such as Bcl-2 and the obstruction of mitochondrial membrane permeabilization.[30] However, upon death stimuli, some apoptogenic factors such as cytochrome c and Smac/Diablo are released and then activate cell apoptotic protease caspase. The activated caspase can positively feedback to attack mitochondria, which lead to a more profound release of cytochrome c and consequently mitochondrial dysfunction including complete disruption of mitochondrial electron transport chain, cellular ROS generation, late stage of apoptotic events, etc.[31] And many key events including the initiation and effectuation of mitochondrial signaling pathway are known to be triggered by Ca^{2+} signals. For instance, Ca^{2+} can not only affect the permeability of mitochondrial membrane but also amplify apoptotic signals through trigger the further cytochrome c release.[32] Therefore, intracellular Ca^{2+} level responded to combination treatment with CNTs and nsEPs was assessed in this study. Results suggested an enhanced plasma membrane permeabilization, which induced a significant Ca^{2+} influx, and then triggered the mitochondrial signaling pathway. The high apoptosis rate of human colon cancer cells presented in our study suggested that the new modality by combining nsEPs with conductive CNTs may be a promising tool for improving the antitumor efficacy.

2. Results and Discussion

2.1. Enhancement of Cell Electropermeabilization around the CNT Tips

As described in the "experimental" section, a FEM model was introduced to theoretically compare the electric field and pore density with and without CNT, moreover, relate the results to membrane permeabilization. **Figure 1**A shows the electric field norm in the region around the CNT and far away from the CNT. A discontinuity in Figure 1A-a was observed due to the different conductivity inside and outside cell membrane which induced a jumped normal component. However, the E_{tip} (electric field at CNT tip) was obviously much stronger than the one at the other side. The value could be several orders of magnitude larger than 4 kV cm^{-1}, which was supposed to be formed in the extracellular area with a low applied voltage. The results suggested CNT's ability to enhance the electric field and form a relatively localized high intensity region at its vicinity due to the special structures of high aspect ratios which induce the "lightening rod effect."[17,19,33] The results of induced pore density by electric field shown in Figure 1B further verified the effect. Pore density at the anodic pole in contact with the CNT tip structure was much higher than the one at the cathodic pole. However, according to the results published by Mao et al., the pore density at the two poles should be the same with each other when there is no CNT around.[34] Thus, it may be the CNT which enhanced the electric field, increasing the transmembrane potential at the contact membrane and ultimately resulting in a much larger pore density. Besides, the pore density induced in the plasma membrane contacted with CNT tip was above 10^{17} m^{-2}, which was much higher than the electroporated threshold, allowing much more molecules to penetrate plasma through the aqueous pores. Considering all the results above, theoretical evidences were provided that CNT could significantly enhance the localized electric field to increase cell plasma membrane permeabilization, which relates to an intensive pore density.

Moreover, cell membrane marker Dio was used to verify the effect of CNTs on membrane perforation when combining with nsEPs in HCT116 cells. The Dio fluorescence showed a green circle along the cell membrane in the control group without treatment in Figure 1C. However, when the cells were exposed to nsEPs (800 ns, 4 kV cm^{-1}, 1 Hz), the Dio fluorescence slightly reduced whereas it was further decreased and the significant weakening was observed when CNTs were utilized in the combined treatment groups, compared to the cells in nsEPs/CNT -treated groups. This trend became much clearer when the fluorescence intensity was quantified as shown in Figure 1D. Significant decrease of the intensity occurred in combination treated groups, compared to the slightly decrease of the Dio signal in nsEPs/CNT-treated groups. Although visible loss of the signal was induced by combination treatment of nsEPs with CNTs, there are some factors that contributing to the weakening fluorescence signals. First, Dio dye formed a good FRET pair with CNTs and was FRET quenched by CNTs. Second, due to its lipophilic hydrophobic feature, Dio dye was easily stacked onto CNTs by hydrophobic interactions or π–π stacking and was carried intracellularly. Third, cell membrane was disrupted when cell was dead because of the Dio toxicity. Finally, the enhanced electric field by nsEPs in the presence of CNTs broke the integrity of cell membrane and thus reduced fluorescence intensity. The first two reasons could be excluded when the cells were treated with CNTs only in present study. The Dio fluorescence in CNT-treated cells was similar with the untreated group, suggesting a low effect of CNTs singly on the fluorescence intensity of Dio dye. Besides, the MTT assay was performed for cells treated with Dio, Dio with CNTs and Dio with nsEPs in the presence of CNTs shown in Supplement 2 (Supporting Information). Results presented a high cell viability when cells were treated with Dio and Dio + CNTs, and there was no difference from that of the untreated cells. This explicitly indicated the low toxicity of Dio to cell. Therefore, the third reason might have low possibility to induce the reduction of Dio fluorescence intensity. Hence, it was inferred that the employment of the CNTs could sufficiently amplify the external nsEPs to induce a considerable formation of the aqueous pores in the biological cell membrane, increasing the cell membrane permeabilization when the simulation results were considered in combination. Besides, the possible reasons for the little differences on Dio fluorescence change between SWNTs, DWNTs, and MWNTs

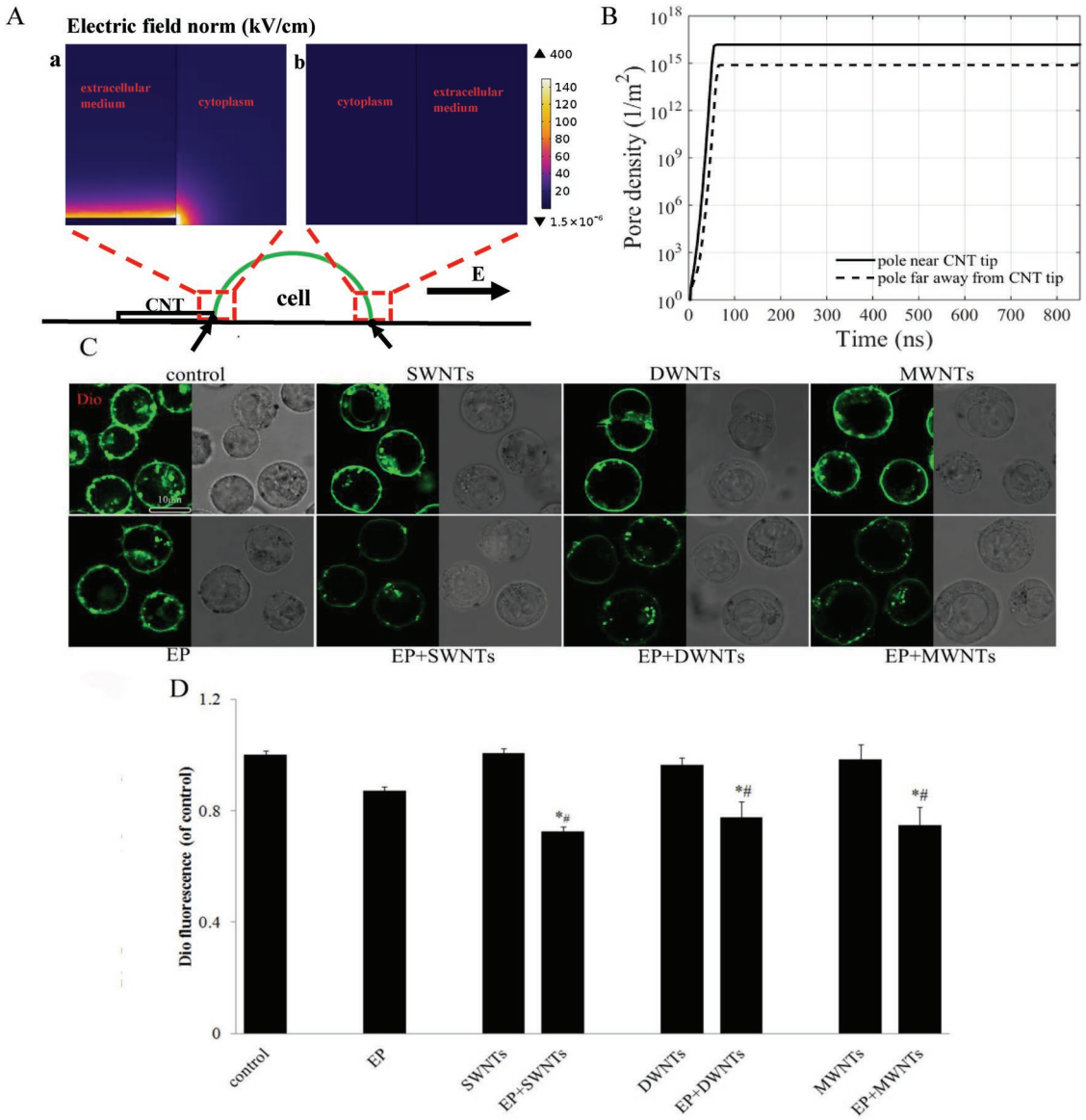

Figure 1. Enhancement of cell electropermeabilization around the CNT tips. A) The electric field distribution around the anodic pole near a) the CNT and the cathodic pole far away from b) the CNT after exposure to 800 ns, 4 kV cm^{-1} nsEP. B) Time evolution of the pore density at the anodic pole and cathodic pole. C) Confocal microscopy images of the cell membrane after HCT116 cells labeled with Dio were treated with nsEPs, 4 μg mL^{-1} CNTs and combination, respectively. D) Statistical analysis of Dio fluorescence in HCT116 cells was performed using spectrofluorometer. Data were presented as the mean ± S.D. ($n = 6$). *$P < 0.05$ versus the single pulse-treated group, #$P < 0.05$ versus the single CNT-treated group as assessed using the one-way ANOVA followed by the Tukey's HSD test.

were suspected to be as follows: 1) As listed in the instructions, the high aspect ratio, that is believed to directly affects the enhancement of electric field,[17,33] between three types of CNTs were similar. And the values were 769, 857, and 833 for SWNT, DWNT, and MWNT, respectively; 2) CNTs' conductivity might also affect the capability of CNT to amplify the electric field. And much higher conductivity of MWNT allows it to accumulate much more electrons at its tip. However, in this study, there were less numbers of MWNT dispersed in the solution of same mass concentration with another two types of CNTs owing to its large size, which might finally result in a similar point response.

2.2. Effects of Combination Treatment on Cell Viability and Proliferation

Effects on cell survival were detected by MTT assay. First, cell viability of the human normal colon epithelial cells NCM460 cell was evaluated when they were exposed to the electric field of 3, 4, and 5 kV cm^{-1} intensity with 600 and 800 ns durations, respectively. As shown in **Figure 2**A, cell survival rate decreased slightly and there was no significant difference between individual nsEP-treated groups and the control group, except for the cells in the groups with electric field of 5 kV cm^{-1} intensity. Furthermore, by comparing the cell viability with exposure of

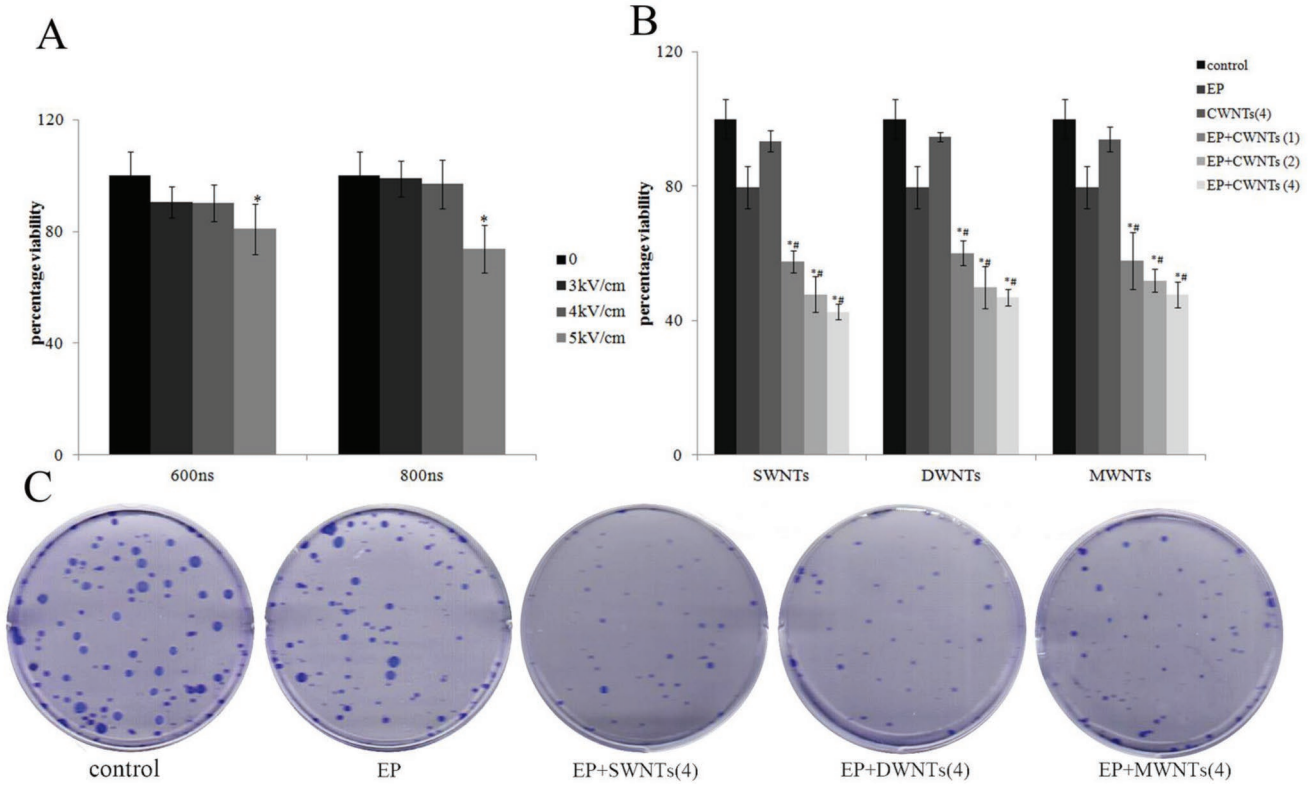

Figure 2. Inhibited cell viability and proliferation caused by the combination treatment with nsEP and CNTs. A) The cell viability of NCM460 cells in individual nsEP-treated groups. Data were presented as mean ± S.D. ($n = 6$). $*P < 0.05$ versus the control group as assessed using the one-way ANOVA followed by the Tukey's HSD test. B) The cell viability of HCT116 cells after treatment with nsEPs, CNTs and combination, the concentration of CNTs was 1, 2, and 4 μg mL^{-1}, respectively. Data were presented as the mean ± S.D. ($n = 6$). $*P < 0.05$ versus the single pulse-treated group, $\#P < 0.05$ versus the single CNT-treated group as assessed using the one-way ANOVA followed by the Tukey's HSD test. C) Representative pictures of colonies stained with crystal violet were obtained using a scanner, the concentration of CNTs in the combined exposure groups were 4 μg mL^{-1}, respectively.

600 and 800 ns durations, slightly more cells survived from the stimulation of 800 ns duration and 3 and 4 kV cm^{-1} intensity. Thus, in order to include a parameter set with minimal toxicity to paired normal cells, an electric field at 4 kV cm^{-1} intensity and 800 ns duration was chosen for the following combination treatments of human colon cancer cells.

Obvious HCT116 cell death was detected when combining nsEPs with three types of CNTs. After treatment for 24 h, nsEPs alone caused about 20% decrease in cell viability and CNTs alone (4 μg mL^{-1}) only caused about 6% cell death. Intriguingly, cell mortality increased sharply when the two treatments were combined. Moreover, the cell survival rate decreased in a dose-dependent manner with the concentrations of CNTs, and the viability percentage decreased to about 40% when the highest concentration of CNTs (4 μg mL^{-1}) were used (Figure 2B). Meanwhile, colony formation assay, another evaluation method of cell growth and proliferation, was performed. As shown in Figure 2C, in the control group, cells divided continuously and formed many colonies. The colony sizes were large enough to be visible when stained by crystal violet. Not surprisingly, with the nsEPs exposure, the number of visible colonies reduced slightly. Nevertheless, cell growth was obviously inhibited and no or only few visible colonies could be found in all nsEPs + CNTs groups (Figure 2C). These results consistently showed that CNTs really enabled higher mortality of HCT116 cells by combined with nsEPs.

2.3. Effects of EP Stimulation Combined with CNTs on Cell Apoptosis

Apoptosis, also known as programmed cell death, is considered a vital component of various processes including normal cell turnover, embryonic development, chemical-induced cell death, tumor chemotherapy, and so on.[35] Herein, Hoechst 33 258 was utilized at 5 min and 2 h after treatment with nsEPs or nsEPs with CNTs to visualize cell apoptosis and the accompanied morphology change using confocal microscopy. As shown in Supplement 1 (Supporting Information), compared to the untreated group and nsEP-treated group, obvious early cell apoptotic morphological changes including chromatic agglutination, karyopyknosis, and nuclear fragmentation were observed in some of the cells from nsEPs+CNTs exposed groups as early as 5 min after treatment. After treatments for 2 h, the Hoechst signal further escalated and higher cell density could be observed. Furthermore, Annexin V/PI double staining was performed at 3 h after treatments to sequentially quantify the cell apoptosis. Cell apoptosis at 3 h after stimulations was mainly in the late stage, which was labeled both by PI and Annexin signals (upper right quadrant). As shown in **Figure 3**, there were few late apoptotic cells (about 9% and 5%) with nsEPs or CNTs treatments. When both agents were included, the percentage of late apoptotic cells increased in a dose-dependent

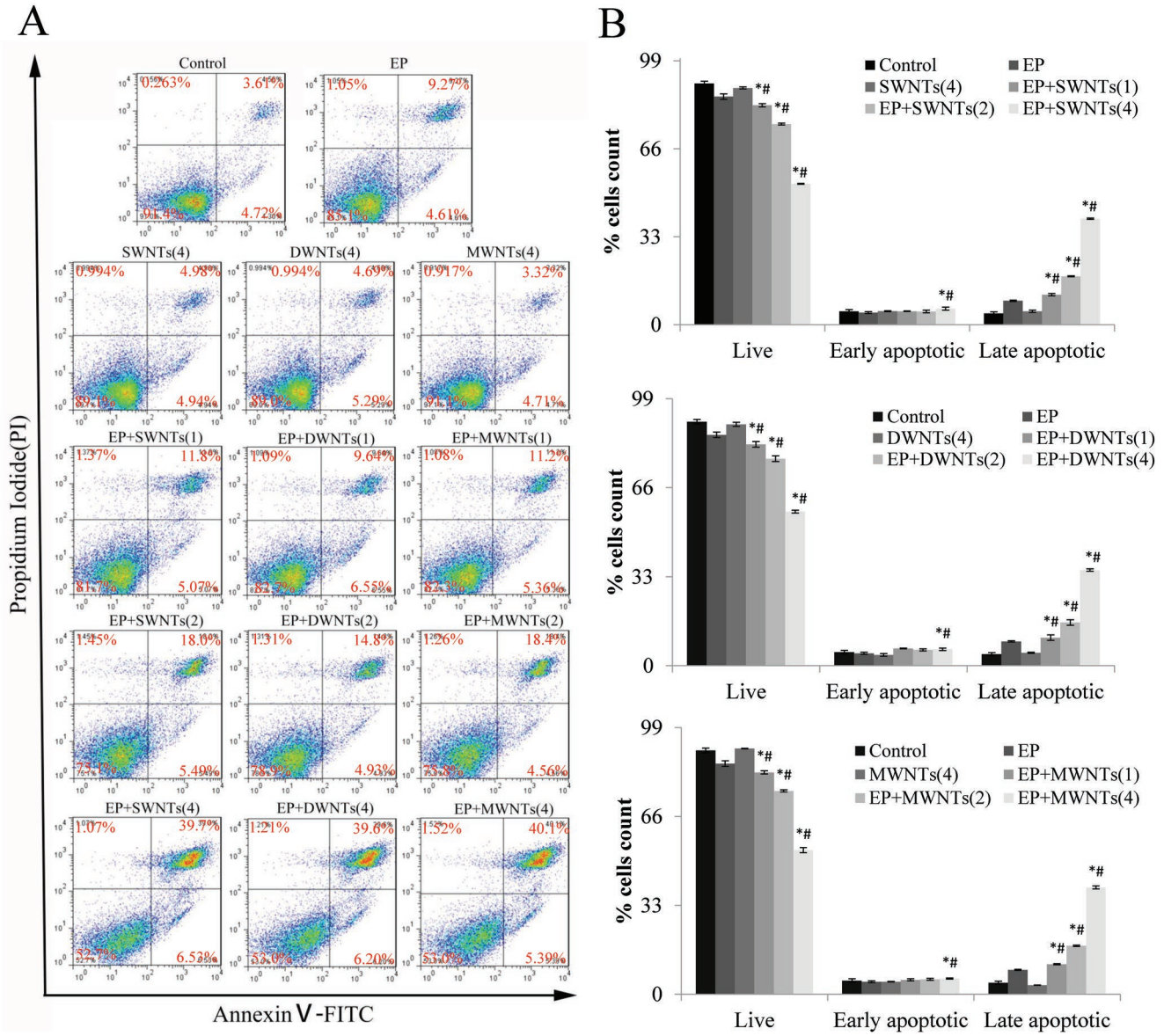

Figure 3. Flow cytometric analysis of apoptosis in HCT116 cells using AnnexinV–FITC/PI staining at 3 h after treatment. Cells were only treated with nsEPs or 4 μg mL^{-1} CNTs, or treated with both nsEPs and CNTs (1, 2, and 4 μg mL^{-1}, respectively). A) Typical figures were shown in quadrants. Cells in the lower right quadrant represent early apoptotic cells, and those in the upper right quadrant represent late apoptotic cells. B) The percentage of apoptotic cells was presented as the mean ± S.D. ($n = 3$). *$P < 0.05$ versus the single pulse-treated group, #$P < 0.05$ versus the single CNT-treated group as assessed using the one-way ANOVA followed by the Tukey's HSD test.

manner following the concentrations of CNTs in all the combination groups, and about 40% late apoptotic cells were detected in combined-treated groups with 4 μg mL^{-1} CNTs (Figure 3). This might result from the enhanced electric field by CNTs. Due to the high aspect ratio and the numerous electron aggregating at the sharp tips of CNTs, surface charge density was sufficiently high, which may induce the specific "lightening rod effect," thereby forming a significantly enhanced electric field at their tips. Published reports showed that high intensity nsEPs were able to induce efficient cell apoptosis in cancer therapy.[11,15,36,37] Although the amplitude of nsEPs in this study was not sufficiently high, due to the amplified electric field by CNTs, the original effects of the nanosecond electric pulses on cell apoptosis induction were ultimately strengthened.

2.4. Morphological and Functional Changes of Mitochondria in Response to EP Stimulation Combined with CNTs

Studies have shown a strong ability of the nanosecond electric pulses to penetrate the plasma membrane and target the intracellular organelles.[15,38] Although compared to the strong electric field (about 80 kV cm^{-1} to MV cm^{-1}) used by Beebe et al., a smaller electric field was applied in the present study to avoid

harmful effects to normal cells,[20,39] we still hypothesized that the combination treatment of nsEPs with CNTs could also affect the organelles, due to the amplified effects of the nsEPs by CNTs. Thus, transmission electron microscope (TEM) was then employed to observe the ultrastructural changes of mitochondria. As shown in **Figure 4**A, in contrast to the intact mitochondria with closely and orderly arranged cristae in untreated cells, the cristae of the HCT116 cells swelled and were ill-defined, and a high electron dense precipitated in the mitochondrial matrix when the HCT116 cells were exposed to nsEPs combined with the three types of CNTs, respectively (Figure 4A). Considering the correlation of the ROS to mitochondrion damage, the production of ROS within the cells was detected by employing a ROS-sensitive fluorometric probe, DCFH-DA. As shown in Figure 4B, a significant ROS generation was observed at 5 min after cells being treated with nsEPs + SWNT, and the DCF fluorescence intensity was about threefolds to that in control group. Reports verified that high level ROS could induce the decrease of mitochondria membrane potential.[40–42] Thus, the mitochondria membrane potential (MMP, $\Delta\varphi_m$) was also evaluated using a potential-dependent J-aggregate forming lipophilic cation (JC-1). The JC-1 aggregated in normal mitochondria and presented red fluorescence in control group as shown in Figure 4C. While nsEPs exposure resulted in slight mitochondria depolarization of $\Delta\varphi_m$ as indicated with the increased green fluorescence in 5 min after treatment. However, additional involvement of the CNTs could significantly decrease $\Delta\varphi_m$. When the cells suspended in CNTs buffers were stimulated by nsEPs, dramatical increases of green fluorescence and little red fluorescence were observed (Figure 4C). After 2 h incubation, the J-aggregates (red) still dominated in the control group, and the $\Delta\varphi_m$ was depolarized more seriously and almost no red fluorescence was detected in response to both the nsEPs and CNTs exposure, suggesting a continuous injury to the mitochondria. The ratio of red and green fluorescence was also calculated to demonstrate the toxicity in mitochondria. CCCP was used as a positive control for $\Delta\varphi_m$ depolarization here, and its values were normalized with the ratio from CCCP. After treatment for 5 min, JC-1 aggregated and the ratio was 4.93 ± 0.37 in untreated cells. The nsEPs treated cells showed a lower ratio, and the lowest values about 2.3 occurred when the cells were exposed to the nsEPs combined with CNTs. The ratio decreased more significantly after incubation for 2 h, and the values were less than 2 in all the EP + CNTs treated groups (Figure 4D). Considering the phenomenon observed by Madani et al. that the carbon nanotubes distributed in cell cytoplasm,[9] the intracellular electric fields might be sufficiently enhanced, which might partly contribute to the dramatical damage of the mitochondria observed in the nsEPs + CNTs groups.

2.5. Effects on the Release of Cytochrome c and Activation of Caspase-9 and -3

The mechanisms of cell apoptosis are highly complex and sophisticated. Mitochondrial pathway is the most common apoptotic mechanism in animal cells, and the mitochondrion is the core of this pathway.[43,44] Research has shown that mitochondrion plays an essential roles in triggering apoptosis through the mitochondrial permeability transition,[45–47] which leads to a loss of $\Delta\varphi_m$ and brings about translocation of pro-apoptotic Bax to mitochondria and cytochrome c from mitochondria to cytosol, also activating the apoptogenic molecules such as caspase-9 and -3.[48,49] The release of cytochrome c is the critical step in the mitochondrial pathway, which triggers the apoptosome formation and initiates the caspase cascade.[36,37] Therefore, the subcellular localization of cytochrome c in nsEP-treated cells with or without CNTs exposure was determined by immunofluorescent labeling, for both the morphological changes of mitochondria and depolarization were observed in the present study. As shown in **Figure 5**A, cytochrome c displayed a dotted pattern located within the mitochondria, corresponding to the red fluorescence (mitochondrion) in untreated cells. However, the staining pattern became diffused in some cells in the nsEP-treated group, which is consistent with a translocation of cytochrome c into the cytosol. Moreover, cytochrome c release became more obvious when cells were treated with both nsEPs and CNTs, as indicated by the ectopic distribution of green fluorescence and red fluorescence (Figure 5A). Furthermore, the activity of caspase-9 and -3 was also examined by colorimetric analysis. As shown in Figure 5C, exposure to nsEPs in the presence of SWNTs remarkably increased activation of caspase-9 and -3 and no significant difference could be observed in all the untreated, SWNT-treated and EP-treated groups. These results indicated that the mitochondrial pathway was involved in the apoptosis induced by the combination treatment with nsEPs and CNTs.

2.6. Effects on Expression of Bcl-2 and Bax

The Bcl-2 family, including proapoptotic factor Bax and Bid, as well as anti-apoptotic proteins Bcl-2 and Bcl-xL, determines the fate of cells in many programmed cell death systems. For instance, Bcl-2 can suppress the mitochondria mediated apoptotic pathway in cancer cells.[30] In addition, Blc-2 expression level and activation stage could also influence the release of cytochrome c, caspase-9 and -3 that further indicated a mitochondrion pathway apoptosis.[31] In our case, Bax and Bcl-2 expression was detected by western blotting. As shown in Figure 5B, the Bax level was obviously upregulated upon the combination treatment of nsEPs with SWNT, and the Bcl-2 expression level was significantly downregulated compared to the untreated, SWNT-treated and EP-treated cells. The imbalance between the two proteins might indicate an undergo apoptosis of cells, which would also promote a number of apoptotic molecules release including cytochrome c, caspase-9 and -3.

2.7. Effects on Ca^{2+} Signaling

Ca^{2+} signaling regulates a variety of cellular functions in multiple cell systems. There are studies indicating that mitochondria generally participate in Ca^{2+} signaling by regulating apoptosis.[50] In this study, mitochondrial Ca^{2+} level was detected using Rhod-2, a specific cell-permeable probe, which is often used to measure the Ca^{2+} levels in mitochondria.[51] In contrast to the weak red fluorescence in the control mitochondria, observable Ca^{2+} accumulation exhibited in the nsEP-treated mitochondria as the increased red fluorescence

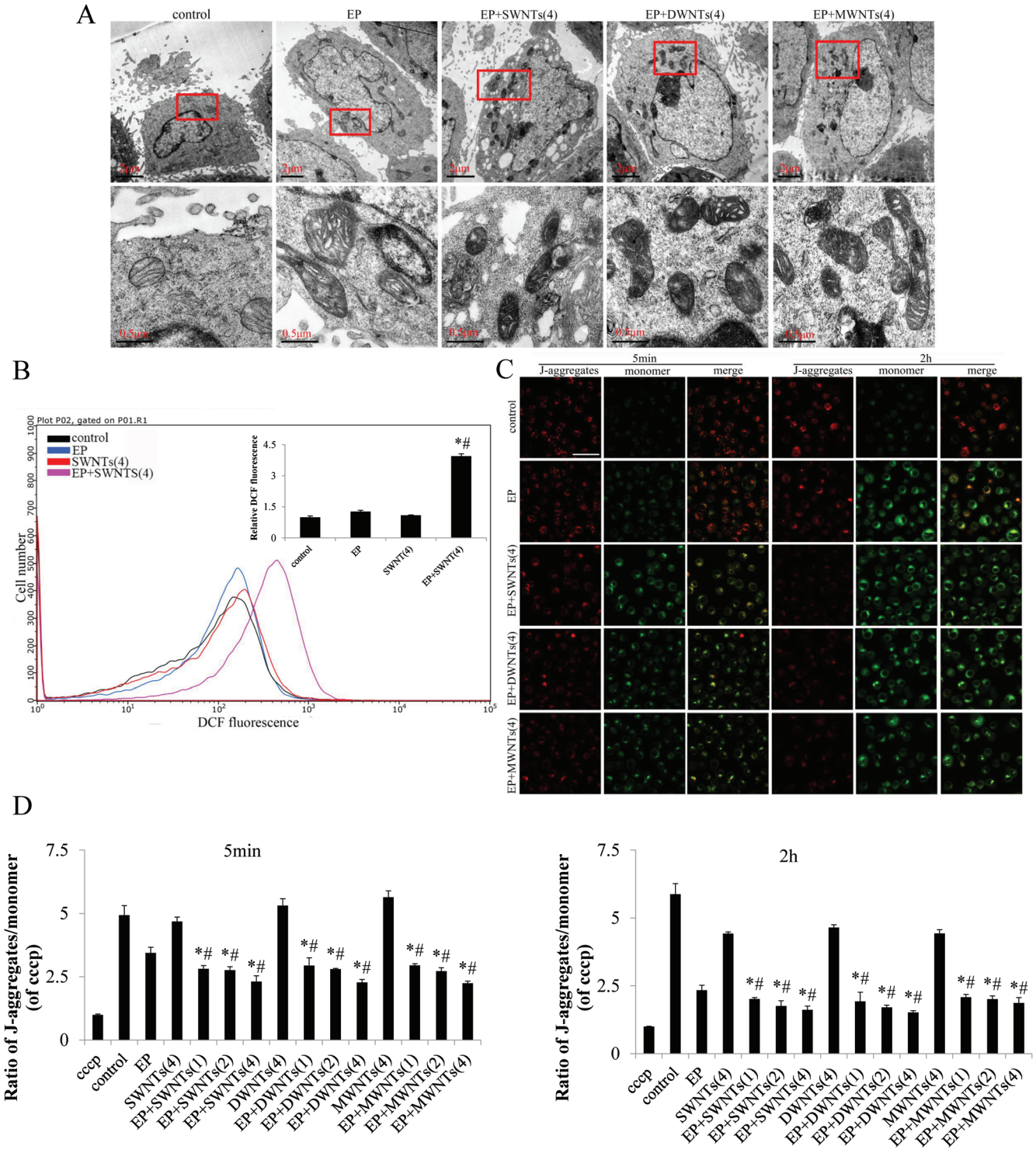

Figure 4. Pathological changes of mitochondria in HCT116 cells after treated in different groups. A) Mitochondria ultrastructure by TEM. B) ROS generation was determined by flow cytometry, and the DCF fluorescence intensity was quantified. Data were presented as the mean ± S.D. ($n = 3$). $^*P < 0.05$ versus the single pulse-treated group, $\#P < 0.05$ versus the single SWNT-treated group as assessed using the one-way ANOVA followed by the Tukey's HSD test. C) Confocal microscopy photographs of mitochondrial membrane potential depolarization (JC-1 staining) caused by combination treatments, bar = 50 μm. D) The red and green fluorescence was quantified using spectrofluorometer, and the ratio of red and green fluorescence was calculated to indicate the changes of mitochondrial membrane potentials. CCCP was used as a positive control for $\Delta\varphi_m$ depolarization here, and values were normalized with the ratio from CCCP. Data were presented as the mean ± S.D. ($n = 6$). $^*P < 0.05$ versus the single pulse-treated group, $\#P < 0.05$ versus the single CNT-treated group as assessed using the one-way ANOVA followed by the Tukey's HSD test.

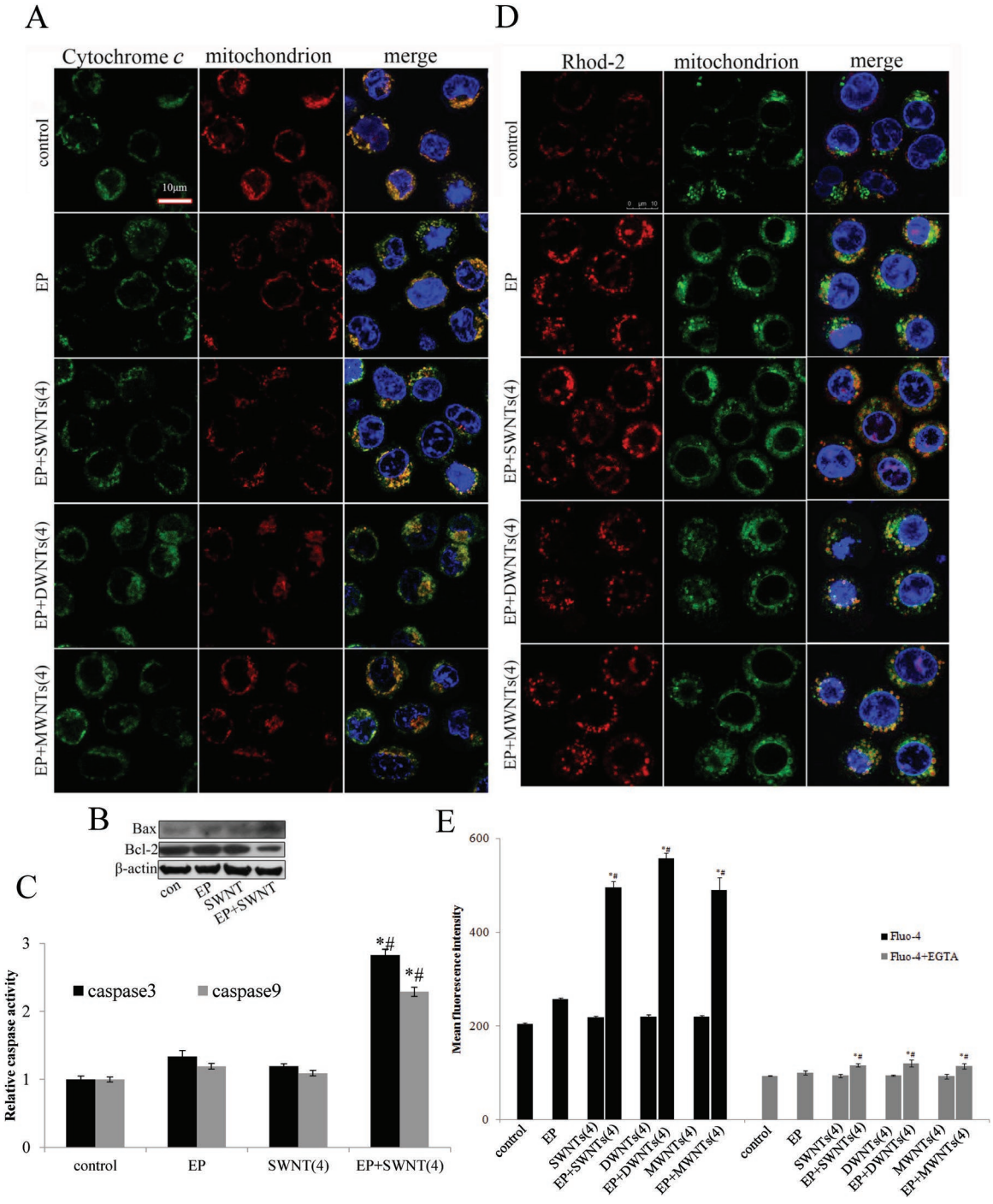

Figure 5. Effects on cytochrome c release and Ca^{2+} handling in HCT116 cells. A) Translocation of cytochrome c from mitochondria to cytosol was observed in response to the combination treatments. Cells were fixed and labeled for cytochrome c (green), mitochondria (red), and nucleus (blue). Images were obtained with a confocal microscope. B) Protein level of Bax and Bcl-2 was determined by western blotting analysis. Total protein of HCT116 cells that treated with nsEPs, SWNT, and combination were extracted after 5 min of nsEPs exposure. The expression level was normalized by β-actin. C) Activities of caspase-3 and -9 were quantified using colorimetric assay. The activity per microgram of protein was presented as fold increase on the basal level (control group cells). Data were presented as the mean ± S.D. ($n = 3$). $^*P < 0.05$ versus the single pulse-treated group, $\#P < 0.05$ versus the single SWNT-treated group as assessed using the one-way ANOVA followed by the Tukey's HSD test. D) Representative microscopic images of Ca^{2+} accumulation in mitochondria test using Rhod-2. Cells were labeled for mitochondrial Ca^{2+} (Rhod-2, red), mitochondria (green) and nucleus (blue), and images were obtained with a confocal microscope. E) Flow cytometric analysis of intracellular Ca^{2+} content in the presence or absence of extracellular Ca^{2+} using Fluo-4/AM. Data were presented as the mean ± S.D. ($n = 3$). $^*P < 0.05$ versus the single pulse-treated group, $\#P < 0.05$ versus the single CNT-treated group as assessed using the one-way ANOVA followed by the Tukey's HSD test.

overlapped with green fluorescence (mitochondria) as shown in Figure 5D. Notably, the Ca^{2+} accumulation in mitochondria became more dramatical after the combination treatment, which may ultimately result in the overload of the mitochondrial Ca^{2+} levels, and then trigger the apoptotic process through inducing cytochrome c release.

Researches have reported that mitochondrial Ca^{2+} signals were directly modulated by members of the Bcl-2 protein family who induce cell apoptosis either by facilitating Ca^{2+} entry into mitochondria through the increased mitochondrial permeability, or through enhancement of Ca^{2+} release from the endoplasmic reticulum (ER).[52] Therefore, in order to further investigate the mechanism of mitochondrial calcium overload caused by combination treatment, cells were loaded with Fluo-4 directly to determine the cytosolic Ca^{2+} level after being treated with nsEPs with or without combining with CNTs as described in the materials and methods section. Figure 5E shows that the cytosolic Ca^{2+} levels dramatically increased in response to the stimulation by electric pulses with CNTs. Although the Ca^{2+} level relatively increased in the group treated with the nsEPs/CNTs, no significant difference was observed until the CNTs were involved. In addition, experiments were also carried out with Fluo-4 in the presence of EGTA to chelate all the extracellular Ca^{2+}. Cytosolic Ca^{2+} levels decreased markedly in all groups compared to that in the presence of extracellular Ca^{2+}, revealing that the calcium influx from extracellular media should be mainly responsible for the increased cytosolic Ca^{2+} levels. However, significant increases of intracellular Ca^{2+} release still could be observed in the combination treatment groups, which suggested that treatment combined with nsEPs and CNTs was also suspected to trigger calcium release from intracellular calcium storages.

Overall, the elevated cytosolic Ca^{2+} levels were speculated to be from two different pathways. On the one hand, the enhanced permeablization of plasma membrane by the combination treatment should be partly responsible. On the other hand, as some reports claimed that Bcl-2 protein family could also participate in the mitochondrial pathway through enhancement of Ca^{2+} release from the ER.[52] In this study, the significant increase of intracellular Ca^{2+} was also observed in the absent of extracellular Ca^{2+}, which together with the decreased Bcl-2/Bax expression ratio might suggest that calcium release from intracellular storages such as ER accounted for the cytosolic Ca^{2+} increase. In addition, ROS and Ca^{2+} are mutually interconnected, wherein ROS can regulate cellular Ca^{2+} influx into the cell and intracellular Ca^{2+} stores, and Ca^{2+} can increase production of the ROS.[53] Moreover, studies also proposed that ROS can act upon the mitochondrion, causing a disruption of $\Delta\varphi_m$ and cytochrome c release.[42,54,55] In this study, intensive ROS production was detected at 5 min after combination treatment were performed, suggesting the involvement of ROS in the combination treatment with nsEPs and CNTs induced cell apoptosis in HCT116 cells. However, the mechanism remains unclear, and further studies are still needed.

3. Conclusion

Searching for a highly efficient and low side-effect method is now quite urgent for cancer therapy. In this study, we proposed a treatment combining low intensity nanosecond electric pulses with CNTs to induce sufficiently high mortality of human colon cancer cells, while on the premise of no CNTs being around, cause little harm to paired healthy colon cells. Results showed the enhanced effects on cell mortality rates in HCT116 cells. The underlying mechanism may be as follows (**Figure 6**): The electric fields were amplified by the CNTs around their tips, thus enhancing the permeabilization of the plasma membrane and then leading to calcium influx. On the other hand, the electric field also triggered Ca^{2+} released from intracellular storages to cytoplasm in a direct/indirect manner. The large increased cytosolic Ca^{2+} then induced the mitochondrial Ca^{2+} uptake and resulted in Ca^{2+} overload, thus causing substructural and functional damage to mitochondria, and ultimately initiating the apoptotic process through the translocation of cytochrome c to cytoplasm and activation of caspase-9 and -3. Besides, ROS generation also involved in the combination treatment induced cell apoptosis. Therefore, the conjugated approach with nsEPs and CNTs might provide an advantageous treatment for human colon cancer in vitro.

4. Experimental Section

FEM Simulation: The finite element method (FEM) was implemented in COMSOL Multiphysics (The COMSOL Group, Stockholm, Sweden) to simulate the enhancement of the CNT on the localized electric field and pore density in cell membranes with the nanosecond electric pulse exposure. The geometric model was axisymmetric. As shown in **Figure 7**, the 100 μm × 50 μm box was constructed with an 8 μm radial cell and a cell-contacted CNT inside. The diameter of the CNT was 10 nm and the length was 10 μm. The four boundary conditions of the box were labeled in the diagram. The electric pulse used to stimulate the cell was 800 ns duration with the amplitude of 4 kV cm^{-1} (V_0 = 400 V). The mathematical equations to calculate the electric field and the pore density could be found in our previous work.[34] Simulation parameters were listed in the **Table 1**.

Preparation of CNTs Pulsing Buffer: Purified CNTs (SWNTs, DWNTs, and MWNTs) were purchased from Sigma-Aldrich (St. Louis, MO, USA). According to the methods of Harada et al.[57] and Lee et al.,[20] CNTs were suspended in mPEG-pyrene solution (5 mg mL^{-1}), and sonicated for 60 min at room temperature, then the CNTs suspensions were centrifuged at 10 000 g for 1 h to remove the residuals. Meanwhile the residuals were collected and dried. Unboned excess mPEG-pyrene in the supernatant were removed by filter tubes (100 kDa AmiconYM-50, Millipore), centrifuged at 4000 rpm for 30 min, and washed thoroughly with distilled water. The stock concentrations of CNTs–PEG were calculated based on the mass of dried CNTs and the volume of CNTs–PEG obtained finally.

Cell Culture and Combination Treatment: Human colon cancer cell line HCT116 and a normal human colon mucosal epithelial cell line NCM460 were purchased from the Institute of Cell Biology (China). Cells were cultured in DMEM medium (Gibco, USA), which was supplemented with 10% fetal bovine serum and penicillin–streptomycin, in a humidified 5% CO_2 atmosphere at 37 °C. When the cells grew to 80% confluence, they were subcultured or used in experiments.

In the EP system, the nsEPs generator was the same as we employed in the previous study.[1] For HCT116 cells, CNTs–PEG stock solution was diluted with PBS to reach final working concentration of 1, 2, and 4 μg mL^{-1}. Cells were harvested and resuspended in CNTs–PEG pulsing buffer to a concentration of 2×10^6 cells mL^{-1}. A total amount of 200 μL cell suspension was placed in cuvettes and exposed to 10 pulses with durations of 800 ns. The electric field strengths were 4 kV cm^{-1}, and pulse repetition frequency was 1 Hz. Three control groups were included in all experiments: cells received neither CNTs nor nsEPs treatment, cells

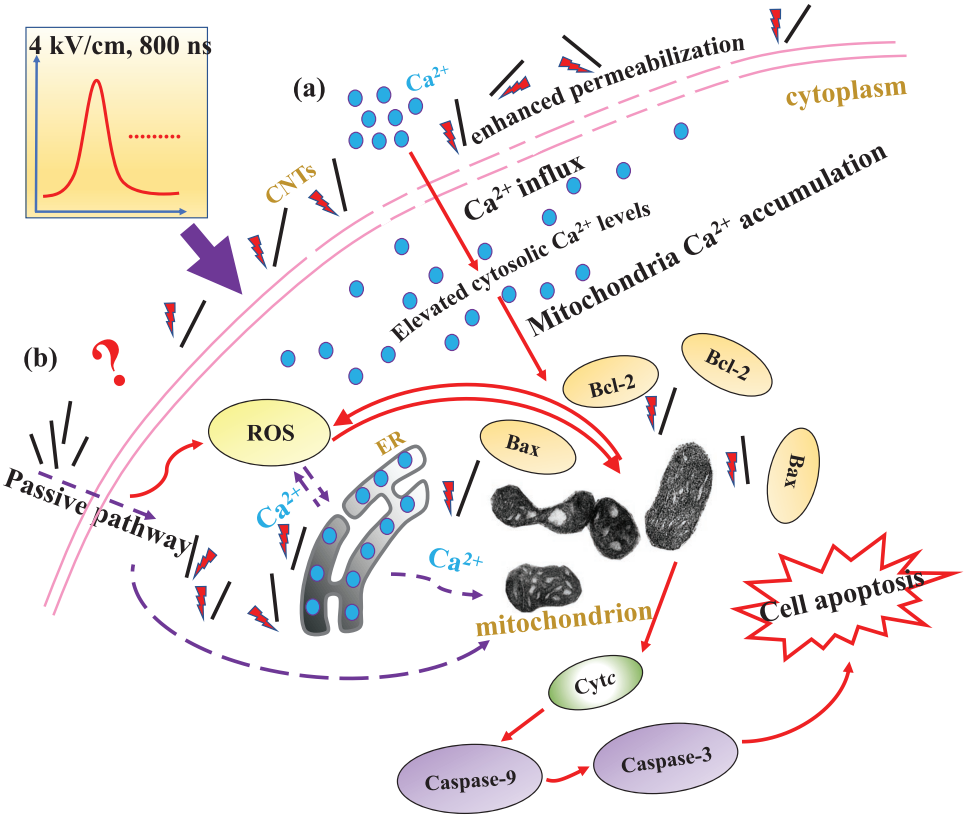

Figure 6. Schematic diagram of mitochondria-mediated apoptosis pathways (initiated by CNTs enhanced plasma membrane permeabilization (a) and intracellular effects (b)) under stimulation of combination treatment (nsEPs + CNTs).

received CNTs (4 µg mL^{-1}) or nsEPs treatment alone. Three replicates of each group were performed. For NCM460 cells, cells were harvested and resuspended in PBS and exposed to 10 pulses with 600, 800 ns durations with electric field of 3, 4, and 5 kV cm^{-1}.

Cell Viability Assay: Cell viabilities were assessed through methyl thiazolyl tetrazolium (MTT) assay as Zhang et al.[58] described. Cells were dispensed into 96-well plates after pulse exposure and cultured with a normal medium for 24 h, and then assayed with MTT. For each sample, there were six replicates. After MTT incubation at 37 °C for 4 h, the culture medium was removed and 150 µL DMSO was added. The optical absorption (OD) values were then determined by spectrophotometry at 490 nm. Cell viability was calculated from the OD values of treated (OD_T) and negative control (OD_C) groups: (OD_T / OD_C) × 100%, respectively.

Colony Formation Assay: After pulse exposure, 500 cells were seeded in each well of a six-well plate, with each group seeded in triplicate. The medium was replaced every 2 d until colony formation was observed. Colonies were fixed with 4% formaldehyde in PBS and stained with 2%

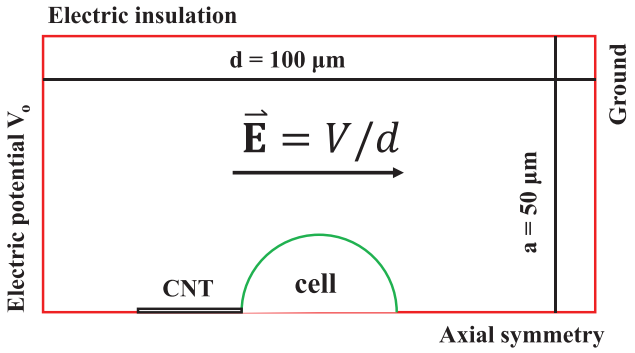

Figure 7. An axially symmetric cell model with carbon nanotube being on the left. The radius of the cell is 8 µm. The diameter of the CNT is 10 nm and the length is 10 µm. The direction of electric field ***E*** is indicated with a bold black arrow. The model is axially symmetric with the bottom (*z*) axis.

Table 1. Model parameters.

Symbol	Value	Description
r_{cell}	8 µm[a)]	Cell radius
d_{CNT}	10 nm	Diameter of carbon nanotube
L_{CNT}	10 µm	Length of carbon nanotube
d_m	5 nm[a)]	Membrane thickness
σ_e	1.2 S m^{-1}[a)]	Extracellular medium conductivity
σ_i	0.5 S m^{-1}[a)]	Intracellular conductivity
σ_m	9.5 × 10^{-9} S m^{-1}[a)]	Membrane conductivity
σ_{CNT}	10^8 S m^{-1}[b)]	Carbon nanotube conductivity
$\varepsilon_e = \varepsilon_i$	72[a)]	Electrolyte relative permittivity
ε_m	5[a)]	Membrane relative permittivity
ε_{CNT}	10[4b)]	Carbon nanotube relative permittivity
σ_p	0.298 S m^{-1}[a)]	Single pore conductivity
r_p	0.8 nm[a)]	Single pore radius
q	1[a)]	Electroporation constant

[a)]Smith and Weaver;[10] [b)]Peng et al.[56]

crystal violet in 2% ethanol. Then photomicrographs of colonies were obtained using a scanner.

Dio Staining: The integrity of plasma membrane was assessed using 3,3′-dioctadecyloxacarbocyanine perchlorate (Dio) according to the method described by Zhang et al.[59] Cells were harvested and incubated with 10×10^{-6} M Dio staining solution, and then observed under a confocal microscope (Leica, Germany) within 5 min after pulsing. Images of green fluorescence and bright-field were obtained.

Apoptosis Assay: Apoptosis at 5 min and 2 h after nsEPs exposure were assessed through Hoechst staining, cells were observed under a confocal microscope (Leica, Germany) and the images were obtained. For the detection of apoptosis at 3 h, cells were dispensed into six-well plates after pulse exposure and cultured in normal media for 3 h. Apoptosis was estimated according to the instructions of the AnnexinV-FITC/PI apoptosis kit (Sigma) by flow cytometry (Merck Millipore, Germany).

Mitochondria Signal Pathway—Measurement of Mitochondrial Membrane Potential: Loss of mitochondrial membrane potential ($\Delta\varphi_m$) was assessed by 5,5′,6,6′-tetrachloro-1,1′,3,3′-tetraethylbenzimidazolecarbocyanideiodine (JC-1; Beyotime, China) staining. Briefly, cells were stained with JC-1staining solution according to the manufacturer's directions. Then cells were observed under a confocal microscope (Leica, Germany) at 5 min and 2 h after pulsing. Images of GFP and RFP were obtained and merged afterwards. Meanwhile, fluorescence intensity of both mitochondrial JC-1 monomers and aggregates were quantified using a Microplate Spectrophotometer. The $\Delta\varphi_m$ of HCT116 cells in each treatment group was calculated as the fluorescence ratio of red (i.e., aggregates) to green (i.e., monomers), and the values were normalized to that of CCCP-treated group (CCCP, carbonyl cyanide m-chlorophenylhydrazone, a protonophore which can cause dissipation of $\Delta\varphi_m$).

Mitochondria Ultrastructure: After pulse exposure, cells were collected and fixed with 2.5% glutaraldehyde for 2–3 h at 4 °C. Samples were then dehydrated and embedded for ultrathin sectioning. The ultrathin sections were stained with uranyl acetate and lead citrate, and then the changes of ultrastructure were observed using transmission electron microscope (Hitachi, Japan), and the images were photographed.

Measurement of Ca^{2+} Signal: The levels of intracellular Ca^{2+} were determined using Flou-4/AM (Beyotime, China). Before pulse exposure, cells were harvested and preincubated with Flou-4/AM in the presence and absence of 5×10^{-9} M EGTA for 60 min at 37 °C. Then cells were exposed to nsEPs with or without CNTs in the pulsing buffer. The Flou-4 fluorescence was determined by flow cytometry (Merck Millipore, Germany). The mitochondria Ca^{2+} content was measured using a specific probe, Rhod-2 (Abcam, Cambridge, MA). Mito-tracker green and DAPI (Beyotime, China) were used to indicate mitochondria and nucleus, respectively. Photomicrographs were obtained using confocal microscope (Leica, Germany).

Release of Cytochrome c: After nsEPs exposure, cells were fixed with 4% formaldehyde and then permeabilized in 1% Triton X-100 for immunofluorescent staining. Unspecific binding was minimized by incubating cells in 2% BSA followed by incubation with the mouse anti cytochrome c (Alexa Fluor 488) antibody (Abcam, Cambridge, MA) over night at 4 °C. Then the mitochondria were stained with mito-tracker-red and the nucleus was stained with DAPI. Images were obtained by confocal laser scanning microscopy (Leica, Germany).

ROS Assay: Intracellular ROS levels were determined using 2,7-dichlorofluorosceindiacetate method.[58] HCT116 cells were loaded with 10×10^{-6} M DCFH-DA and incubated at 37 °C for 30 min. Then cells were washed with PBS and treated with nsEPs, SWNT and combination ($n = 3$ per treatment). Flow-cytometric analysis was performed at 5 min after treatments, respectively.

Caspase activity: The activities of caspase-3 and caspase-9 were measured by cleavage of chromogenic caspase substrates, Ac-DEVD-pNA (acetyl-Asp–Glu–Val–Asp p-nitroanilide) and Ac-LEHD-pNA (acetyl-Leu–Glu–His–Asp p-nitroanilide) using the assay kits (Beyotime Biotech. Haimen, China) in accordance with the instructions for use. Briefly, total protein of HCT116 cells that treated with nsEPs, SWNT and both two agents ($n = 3$ per treatment) were extracted at 30 min after each stimulation. Caspase 3 and caspase 9 activities were measured at 405 nm on a microplate reader. In addition, the concentrations of total protein were measured through Bradford method. The activity per microgram of protein was presented as fold increase on the basal level (control group cells).

Western Blot Analysis: Protein expression levels of Bcl-2 and Bax were measured using western blot in accordance with the method described previously.[58] Briefly, total protein of HCT116 cells that treated with nsEPs, SWNT and both two agents ($n = 3$ per treatment) were extracted at 5 min after each stimulation and used for the subsequent steps. Rabbit anti-Bcl-2 and anti-Bax (Abcam, Cambridge, MA) antibodies were used, and the expression levels were presented as relative expression normalized by β-actin (Sigma).

Statistical Analysis: Means and standard deviations of means (SD) were calculated from individual values, and factorial ANOVA followed by the Tukey's HSD test via SPSS 13.0 was used to determine statistical significance. Data are presented as mean ± S.D., and differences were considered significant at $p < 0.05$.

Supporting Information

Supporting Information is available from the Wiley Online Library or from the author.

Acknowledgements

This work was supported by grants from The National Natural Science Foundation of China under contract No. 41390453, and by the Shenzhen Science and Technology Project (JCYJ20180306173301083).

Conflict of Interest

The authors declare no conflict of interest.

Keywords

calcium levels, carbon nanotubes, enhanced electric fields, mitochondria-mediated apoptosis pathway, nanosecond electric pulses

Received: July 25, 2019
Revised: November 6, 2019
Published online: December 4, 2019

[1] Y. Zhang, Z. Mao, B. Wang, J. Zhang, N. Lu, R. Hong, S. Dong, C. Yao, Q. H. Liu, *IEEE Trans. Biomed. Eng.* **2019**, *66*, 3129.
[2] Y. Zhan, C. Sun, Z. Cao, N. Bao, J. Xing, C. Lu, *Anal. Chem.* **2012**, *84*, 8102.
[3] Y. Granot, B. Rubinsky, *Int. J. Heat Mass Transfer* **2008**, *51*, 5610.
[4] P. Mukherjee, S. S. P. Nathamgari, J. A. Kessler, H. D. Espinosa, *ACS Nano* **2018**, *12*, 12118.
[5] B. Markelc, E. Skvarca, T. Dolinsek, V. P. Kloboves, A. Coer, G. Sersa, M. Cemazar, *Bioelectrochemistry* **2015**, *103*, 111.
[6] M. Kandušer, D. Miklavčič, M. Pavlin, *Bioelectrochemistry* **2009**, *74*, 265.
[7] S. Šatkauskas, D. Batiuškaitė, S. Šalomskaitė-Davalgienė, M. S. Venslauskas, *Bioelectrochemistry* **2005**, *65*, 105.
[8] T. B. Napotnik, Y. H. Wu, M. A. Gundersen, D. Miklavčič, P. T. Vernier, *Bioelectromagnetics* **2012**, *33*, 257.
[9] S. Y. Madani, N. Naderi, O. Dissanayake, A. Tan, A. M. Seifalian, *Int. J. Nanomed.* **2011**, *6*, 2963.
[10] K. C. Smith, J. C. Weaver, *Biophys. J.* **2008**, *95*, 1547.

[11] W. Ren, S. J. Beebe, *Apoptosis* **2011**, *16*, 382.
[12] E. H. Hall, K. H. Schoenbach, S. J. Beebe, *Apoptosis* **2007**, *12*, 1721.
[13] S. J. Beebe, P. M. Fox, L. J. Rec, E. L. K. Willis, K. H. Schoenbach, *FASEB J.* **2003**, *17*, 1493.
[14] G. L. Thompson, C. C. Roth, M. A. Kuipers, G. P. Tolstykh, H. T. Beier, B. L. Ibey, *Biochem. Biophys. Res. Commun.* **2016**, *470*, 35.
[15] T. B. Napotnik, M. Reberšek, P. T. Vernier, B. Mali, D. Miklavčič, *Bioelectrochemistry* **2016**, *110*, 1.
[16] H. J. Li, W. Lu, J. Li, X. Bai, C. Gu, *Phys. Rev. Lett.* **2005**, *95*, 086601.
[17] B. Kozinsky, N. Marzari, *Phys. Rev. Lett.* **2006**, *96*, 166801.
[18] J. A. Rojas-Chapana, M. A. Correa-Duarte, Z. Ren, K. Kempa, M. Giersig, *Nano Lett.* **2004**, *4*, 985.
[19] Z.-Y. Huo, Y. Luo, X. Xie, C. Feng, K. Jiang, J. Wang, H.-Y. Hu, *Environ. Sci.: Nano* **2017**, *4*, 2010.
[20] P.-C. Lee, C.-L. Peng, M.-J. Shieh, *J. Controlled Release* **2016**, *225*, 140.
[21] L. Wang, D. Liu, R. Zhou, Z. Wang, A. Cuschieri, *Int. J. Mol. Sci.* **2015**, *16*, 6890.
[22] M. Stacey, C. Osgood, B. S. Kalluri, W. Cao, H. Elsayed-Ali, T. Abdel-Fattah, *Biomed. Mater.* **2011**, *6*, 011002.
[23] V. Raffa, L. Gherardini, O. Vittorio, G. Bardi, A. Ziaei, T. Pizzorusso, C. Riggio, S. Nitodas, T. Karachalios, K. T. Al-Jamal, *Nanomedicine* **2011**, *6*, 1709.
[24] V. Raffa, G. Ciofani, O. Vittorio, V. Pensabene, A. Cuschieri, *Bioelectrochemistry* **2010**, *79*, 136.
[25] B. R. Smith, E. E. B. Ghosn, H. Rallapalli, J. A. Prescher, T. Larson, L. A. Herzenberg, S. S. Gambhir, *Nat. Nanotechnol.* **2014**, *9*, 481.
[26] W. Zhang, Z. Zhang, Y. Zhang, *Nanoscale Res. Lett.* **2011**, *6*, 555.
[27] J. G. Huang, T. Leshuk, F. X. Gu, *Nano Today* **2011**, *6*, 478.
[28] P. D. Kadam, H. H. Chuan, *Int. Urogynecol. J.* **2016**, *27*, 505.
[29] D. C. Wallace, *Nat. Rev. Cancer* **2012**, *12*, 685.
[30] E. Zhang, C. Zhang, Y. Su, T. Cheng, C. Shi, *Drug Discovery Today* **2011**, *16*, 140.
[31] S. Desagher, J.-C. Martinou, *Trends Cell Biol.* **2000**, *10*, 369.
[32] S. Orrenius, V. Gogvadze, B. Zhivotovsky, *Biochem. Biophys. Res. Commun.* **2015**, *460*, 72.
[33] G. S. Bocharov, A. V. Eletskii, *Nanomaterials* **2013**, *3*, 393.
[34] Z. Mao, L. Liu, Y. Zhang, J. Zhang, N. Liu, Q. H. Liu, *IEEE J. Multiscale Multiphys. Comput. Tech.* **2018**, *3*, 235.
[35] S. Elmore, *Toxicol. Pathol.* **2007**, *35*, 495.
[36] P. Simonis, S. Kersulis, V. Stankevich, V. Kaseta, E. Lastauskiene, A. Stirke, *Bioelectrochemistry* **2017**, *115*, 19.
[37] L. He, D. Xiao, J. Feng, C. Yao, L. Tang, *Med. Oncol.* **2017**, *34*, 24.
[38] A. T. Esser, K. C. Smith, T. Gowrishankar, Z. Vasilkoski, J. C. Weaver, *Biophys. J.* **2010**, *98*, 2506.
[39] H. Qiu, S. Xiao, R. P. Joshi, *IEEE Trans. Plasma Sci.* **2014**, *42*, 3113.
[40] Y. Tan, Y. Zhu, Y. Zhao, L. Wen, T. Meng, X. Liu, X. Yang, S. Dai, H. Yuan, F. Hu, *Biomaterials* **2018**, *154*, 169.
[41] G. Wei, Y. Wang, X. Huang, J. Zhao, G. Yang, S. Zhou, *J. Mater. Chem. B* **2018**, *6*, 8137.
[42] L. W. Gao, J. Zhang, W. H. Yang, B. Wang, J. W. Wang, *Toxicol. In Vitro* **2011**, *25*, 51.
[43] L. Ravagnan, T. Roumier, G. Kroemer, *J. Cell. Physiol.* **2002**, *192*, 131.
[44] D. R. Green, J. C. Reed, *Science* **1998**, *281*, 1309.
[45] D.-X. Hou, X. Tong, N. Terahara, D. Luo, M. Fujii, *Arch. Biochem. Biophys.* **2005**, *440*, 101.
[46] H. Ka, H.-J. Park, H.-J. Jung, J.-W. Choi, K.-S. Cho, J. Ha, K.-T. Lee, *Cancer Lett.* **2003**, *196*, 143.
[47] N. Zamzami, P. Marchetti, M. Castedo, D. Decaudin, A. Macho, T. Hirsch, S. A. Susin, P. X. Petit, B. Mignotte, G. Kroemer, *J. Exp. Med.* **1995**, *182*, 367.
[48] J. Chipuk, L. Bouchier-Hayes, D. Green, *Cell Death Differ.* **2006**, *13*, 1396.
[49] X. Jiang, X. Wang, *J. Biol. Chem.* **2000**, *275*, 31199.
[50] O. M. De Brito, L. Scorrano, *Nature* **2008**, *456*, 605.
[51] R. I. Fonteriz, S. de la Fuente, A. Moreno, C. D. Lobatón, M. Montero, J. Alvarez, *Cell Calcium* **2010**, *48*, 61.
[52] Y. Rong, C. W. Distelhorst, *Annu. Rev. Physiol.* **2008**, *70*, 73.
[53] A. Görlach, K. Bertram, S. Hudecova, O. Krizanova, *Redox Biol.* **2015**, *6*, 260.
[54] J.-H. Lee, Y.-S. Won, K.-H. Park, M.-K. Lee, H. Tachibana, K. Yamada, K.-I. Seo, *Apoptosis* **2012**, *17*, 1275.
[55] Y. Tan, Y. Zhu, L. Wen, X. Yang, X. Liu, T. Meng, S. Dai, Y. Ping, H. Yuan, F. Hu, *Theranostics* **2019**, *9*, 691.
[56] N. Peng, Q. Zhang, Y. Sun, *Int. J. Nanomanuf.* **2008**, *2*, 50.
[57] A. Harada, A. Hashidzume, H. Yamaguchi, Y. Takashima, *Chem. Rev.* **2009**, *109*, 5974.
[58] Y. Zhang, L. Huang, Y. Zhao, T. Hu, *Chemosphere* **2017**, *168*, 1506.
[59] Z. Zhang, X. Xiong, J. Wan, L. Xiao, L. Gan, Y. Feng, H. Xu, X. Yang, *Biomaterials* **2012**, *33*, 7233.